

## High Voltage Gain Converter Using an LC Parallel Resonant Tank

Y.Alekhya, B.E

Chaitanya Bharathi Institute of Technology.

T.Pallavi, B.E

Chaitanya Bharathi Institute of Technology.

### Abstract:

With the quick advancement of expansive scale renewable energy sources and HVDC lattice, it is a promising choice to associate the renewable vitality sources to the HVDC framework with an unadulterated dc framework, in which high-control high-voltage venture up dc-dc converters are the key gear to transmit the electrical vitality. This paper proposes a resounding converter which is appropriate for matrix associated renewable vitality sources. The converter can accomplish high voltage pick up utilizing a LC parallel full tank. It is described by zero-voltage-exchanging (ZVS) turn-on and about ZVS turn-off of fundamental switches and additionally zero-current-exchanging turn-off of rectifier diodes; besides, the identical voltage anxiety of the semiconductor gadgets is lower than other full stride up converters. The operation standard of the converter and its full parameter choice is displayed in this paper. The operation guideline of the proposed converter has been effectively confirmed by reproduction and test comes about.

**Index Terms:** Renewable energy, resonant converter, soft switching, voltage step-up, voltage stress.

### I. INTRODUCTION:

The advancement of renewable vitality sources is essential to soothe the weights of weariness of the fossil fuel and en-vironmental contamination. At present, a large portion of the renewable vitality sources are used with the type of air conditioning power. The era types of gear of the renewable vitality sources and vitality stockpiling gadgets more often than not contain dc change stages and the created electrical vitality is conveyed to the force network through dc/air conditioning stages, bringing about extra vitality misfortune.

Additionally, the com-mon issue of the renewable vitality sources, for example, wind and sun based, is the substantial varieties of yield force, and the connection of vast size of the renewable sources to the force framework is a colossal test for the conventional electrical gear, network structure, and operation. DC network, as one of the answers for the previously mentioned issues, is a developing and promising methodology which has drawn much consideration as of late [1]-[4]. At present, the voltages over the dc stages in the era supplies of the renewable vitality sources are moderately low, in the scope of a few hundred volts to a few thousand volts; subsequently, high-control high-voltage venture up dc-dc converters are required to convey the created electrical vitality to the HVDC lattice.

Moreover, as the connectors between the renewable vitality sources and HVDC lattice, the progression up dc-dc converters transmit electrical vitality, as well as confine or buff sorts of deficiency conditions; they are one of the key types of gear in the dc framework [5]. As of late, the powerful high-voltage venture up dc-dc con-verters have been concentrated widely [5]-[29]. The transformer is a helpful way to deal with acknowledge voltage venture up. The clas-sic full-connect (FB) converter, single dynamic scaffold (SAB) con-verter, and LCC thunderous converter are examined and their per-formance is thought about for the seaward wind ranch application [7]-[10]. The three-stage topologies, for example, three-stage SAB converter, arrangement full converter, and double dynamic scaffold con-verter, which are more appropriate for high-control applications because of lightened current anxiety of every extension, are additionally examined and intended for high-control high-voltage venture up applications [11]-[13].

The developing secluded dc–dc converter, which utilizes two particular multilevel converters connected by a medium-recurrence transformer, is appropriate for the application in the HVDC framework [14]–[16]. For these segregated topologies, the fundamental deterrent is the creation of the powerful high-voltage medium-recurrence transformer and there is no report about the transformer model yet. Different little limit separated con-verters associated in arrangement and/or parallel to frame a powerful high-voltage converter is a successful intends to keep away from the utilization of single extensive limit transformer [17]–[20]. For the application where galvanic separation is not mandatory, the utilization of a transformer would just build the cost, volume, and misfortunes, particularly for high-influence high-voltage ap-plications [21].

A few nonisolated topologies for high-control high-voltage applications have as of late been proposed and stud-ied in the writing [21]–[29]. A support converter is adjusted by the scientists of Converteam organization to transmit vitality from  $\pm 50$  to  $\pm 200$  kV [22]. To acquire the higher voltage pick up, Enjeti et al. proposed a numerous module structure, which comprises of aboost converter and a buck/support converter associated in info parallel yield arrangement [23]. The yield force and voltage are shared by the two converters and the voltage and current appraisals of switches and diodes are correspondingly decreased. Be that as it may, the proficiency of a help or buck/support converter is moderately.

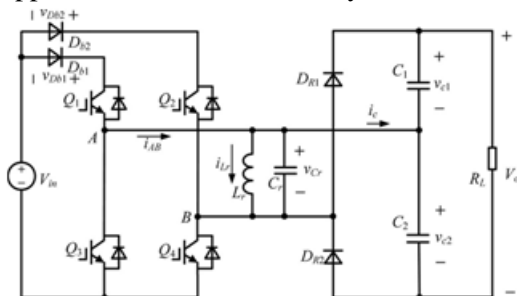


**Fig. 1. Topology of the proposed resonant step-up converter.**

low due to the hard switching of the active switch and the large reverse recovery loss of the diode.

The delicate exchanging innovation is basic to enhance the transformation effectiveness, particularly for high-voltage applications [31]–[37]. As of late, a few delicate exchanging topologies for high-control high-voltage applications have been proposed. In [24] and [25], the converter topologies in light of thunderous exchanged capacitor (RSC) are proposed with diminished exchanging misfortune and secluded structure. The deficiency of the RSC-based converter is the poor voltage direction and the necessity of a vast num-ber of capacitors. Jovic et al. proposed a novel kind of reso-nant venture up converter with conceivably delicate exchanging operation, which uses thyristors as switches and does not experience the ill effects of exorbitant switch hassles and turn around recuperation issues; more-more than, a substantial voltage addition is effortlessly acquired [26]–[28].

Correspondingly, in [29], another group of full transformerless secluded dc– dc converters is proposed and the principle highlight of the proposed converters is that the unequal voltage weight on semiconductors of thyristor valve is kept away from with the utilization of dynamic exchanging net-work, which is made out of an air conditioner capacitor and four indistinct element switches. Thyristors have broad voltage and current ratings; in any case, the usage of thyristor limits the trading repeat of the converter, bringing about cumbersome aloof segments and moderate element reaction [30].

Additionally, the full inductors of the converters are unidirectional polarized in [26]–[29], prompting lower usage of the attractive center, which implies that an incredible volume of center is required. In this paper, a novel resounding stride up dc–dc converter is proposed, which not just can understand delicate exchanging for primary switches and diodes and expansive voltage pick up, additionally has rel-atively bring down identical voltage anxiety of the semiconductor gadgets and bidirectional charged full inductor. The operation eration rule of the converter and the configuration of the resounding parameters are exhibited in this paper.

A 100 V ( $\pm 20\%$ )/1000 V, 1-kW model is inherent the lab to check the successful ness of the converter.

## II. CONVERTER STRUCTURE AND OPERATION PRINCIPLE:

The proposed resonant step-up converter is shown in Fig. 1. The converter is composed of an FB switch network, which com-

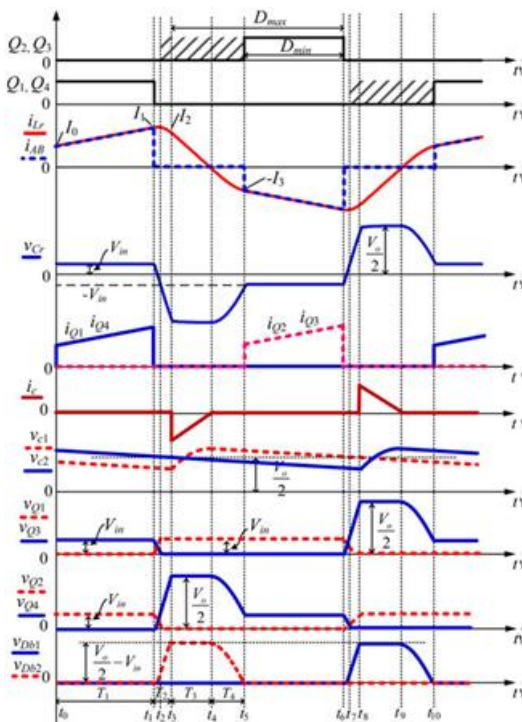


**Fig. 2. Operating waveforms of the proposed converter.**

prises Q1 through Q4 , a LC parallel full tank, a voltage doubler rectifier, and two information blocking diodes, Db1 and Db2 . The unfaltering state working waveforms are appeared in Fig. 2 and point by point operation methods of the proposed converter are appeared in Fig. 3. For the proposed converter, Q2 and Q3 are tuned on and off all the while; Q1 and Q4 are tuned on and off simul-taneously. With a specific end goal to improve the investigation of the converter, the accompanying suspicions are made:

- 1) all switches, diodes, inductor, and capacitor are ideal com-ponents;

- 2) output filter capacitors  $C_1$  and  $C_2$  are equal and large enough so that the output voltage  $V_o$  is considered constant in a switching period  $T_s$  .

### A. Mode 1 [ $t_0$ , $t_1$ ] [See Fig. 3(a)]

Amid this mode, Q1 and Q4 are turned on bringing about the positive information voltage  $V_{in}$  over the LC parallel full tank, i.e.,  $v_L r = v_C r = V_{in}$  . The converter works like an ordinary support converter and the full inductor  $L_r$  goes about as the help inductor with the current through it expanding directly from  $I_0$  . The heap is controlled by  $C_1$  and  $C_2$  . At  $t_1$  , the resounding inductor current  $iL r$  achieves  $I_1$

$$I_1 = I_0 + \frac{V_{in} T_1}{L_r} \quad (1)$$

Where  $T_1$  is the time interval of  $t_0$  to  $t_1$  .

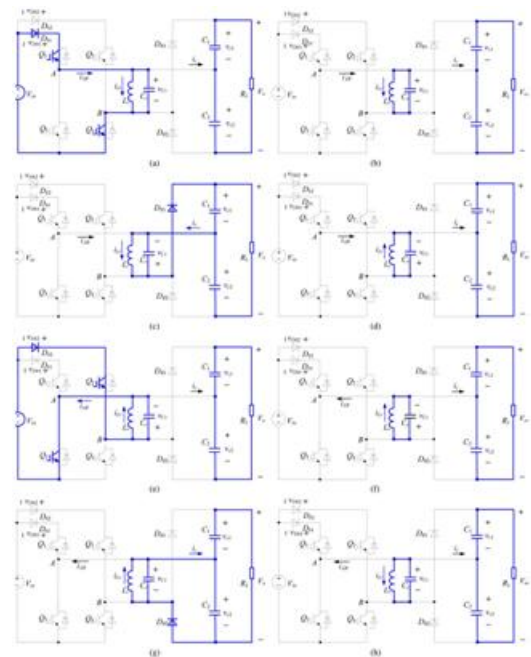


**Fig. 3. Equivalent circuits of each operation stages. (a) [ $t_0$  ,  $t_1$  ]. (b) [ $t_1$  ,  $t_3$  ]. (c) [ $t_3$  ,  $t_4$  ]. (d) [ $t_4$  ,  $t_5$  ]. (e) [ $t_5$  ,  $t_6$  ]. (f) [ $t_6$  ,  $t_8$  ]. (g) [ $t_8$  ,  $t_9$  ]. (h) [ $t_9$  ,  $t_{10}$  ].**

### B. Mode 2 [ $t_1$ , $t_3$ ] [See Fig. 3(b)]

At  $t_1$  ,Q1 and Q4 are turned off and after that  $L_r$  resonates with  $C_r$  ,  $v_C r$  decreases from  $V_{in}$  , and  $iL r$  increases from  $I_1$  in resonant form. Taking into account the parasitic out.

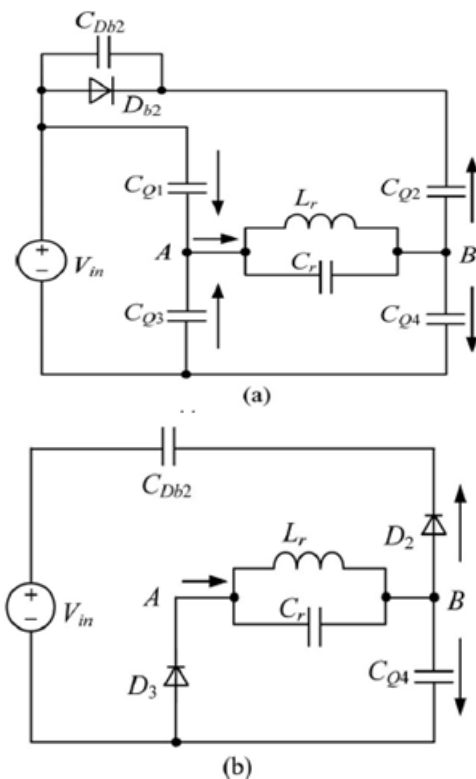


Fig. 4. Further equivalent circuits of Mode 2. (a)  $[t_1, t_2]$ . (b)  $[t_2, t_3]$ .

capacitors of Q1 through Q4 and intersection capacitor of Db2, the proportionate circuit of the converter after  $t_1$  is appeared in Fig. 4(a), in which  $C_{Db2}$ ,  $C_{Q1}$ , and  $C_{Q4}$  are charged,  $C_{Q2}$  and  $C_{Q3}$  are released. Keeping in mind the end goal to acknowledge zero-voltage exchanging (ZVS) for Q2 and Q3, an extra capacitor, whose greatness is about ten times as for  $C_{Q2}$ , is associated in parallel with  $D_{b2}$ . Consequently, the voltage crosswise over  $D_{b2}$  is viewed as unaltered during the charging/releasing procedure and  $D_{b2}$  is identical to be shorted. Because of  $C_r$  is much bigger than the parasitic capacitances, the voltages crosswise over Q1 and Q4 increment gradually. Thus, Q1 and Q4 are killed at just about zero voltage in this mode. At the point when  $v_{C_r}$  drops to zero,  $i_{L_r}$  achieves its greatest extent. After that,  $v_{C_r}$  increments in negative course and  $i_{L_r}$  decreases in thunderous structure. At  $t_2$ ,  $v_{C_r} = -V_{in}$ , the voltages crosswise over Q1 and Q4 reach  $V_{in}$ , the voltages crosswise over Q2 and Q3 fall to zero and the two switches can be turned on

under zero-voltage condition. It ought to be noted that although Q2 and Q3 could be turned on after  $t_2$ , there are no streams coursing through them. After  $t_2$ ,  $L_r$  continues to reverberate with  $C_r$ ,  $v_{C_r}$  increases in negative direction from  $-V_{in}$ ,  $i_{L_r}$  decreases in resounding structure.  $D_{b2}$  will hold turned around predisposition voltage and the voltage crosswise over Q4 keeps on expanding from  $V_{in}$ . The voltage crosswise over Q1 is kept at  $V_{in}$ . The identical circuit of the converter after  $t_2$  is appeared in Fig. 4(b), in which  $D_2$  and  $D_3$  are the antiparallel diodes of Q2 and Q3, individually. This mode keeps running until  $v_{C_r}$  increments to  $-V_o/2$  and  $i_{L_r}$  reduces to  $I_2$ , at  $t_3$ , the voltage crosswise over Q4 reaches  $V_o/2$  and the voltage crosswise over  $D_{b2}$  achieves  $V_o/2 - V_{in}$ . It can be seen that amid  $t_1$  to  $t_3$ , no force is exchanged from the info source or to the heap, and the whole energy stored in the LC resonant tank is unchanged, i.e.,

$$\frac{1}{2} L_r I_1^2 + \frac{1}{2} C_r V_{in}^2 = \frac{1}{2} L_r I_2^2 + \frac{1}{2} C_r V_o^2 \quad (3)$$

#### D. Mode 4 $[t_4, t_5]$ [See Fig. 3(d)]

At  $t_4$ ,  $i_{L_r}$  reductions to zero and the present coursing through  $D_{r1}$  also abatements to zero, and  $D_{r1}$  is killed with zero-current exchanging (ZCS); along these lines, there is no opposite recuperation. After  $t_4$ ,  $L_r$  reverberates with  $C_r$ ,  $C_r$  is released through  $L_r$ ,  $v_{C_r}$  increments from  $-V_o/2$  in positive course, and  $i_{L_r}$  increments from zero in negative heading. In the interim, the voltage crosswise over Q4 declines from  $V_o/2$ . At  $t_5$ ,  $v_{C_r} = -V_{in}$ , and  $i_{L_r} = -I_3$ . In  $t_5$

TABLE I  
COMPARISON OF DIFFERENT NONISOLATED CONVERTER TOPOLOGIES

Topologies	Voltage stress	Soft switching	Voltage regulation	Switching frequency	Output fault shorts output	Input fault shorts output
Ref.[22], [23]	Low	No	Good	Constant	Yes	No
Ref.[24], [25]	Low	Yes	Poor	Constant	Yes	Yes
Ref.[26]-[28]	High	Yes	Good	Variable	No	No
Ref.[29]	High	Yes	Good	Variable	Yes	No
Proposed one	Medium	Yes	Good	Variable	No	No

Fig. 5. Voltage gain versus  $\omega_r$  and  $T_4$ .

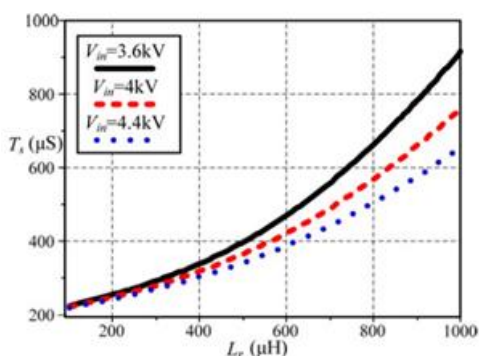


Fig. 6. Curves between  $L_r$  and  $T_s$  under different input voltages.

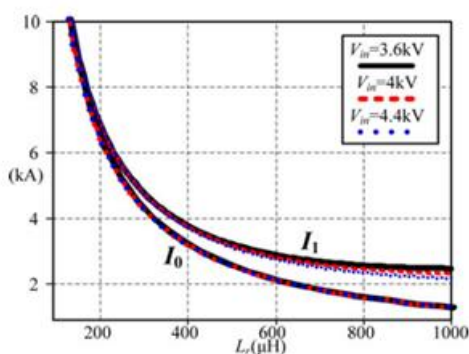


Fig. 7. Curves between  $L_r$  and  $I_0$ ,  $I_1$  under different input voltages.

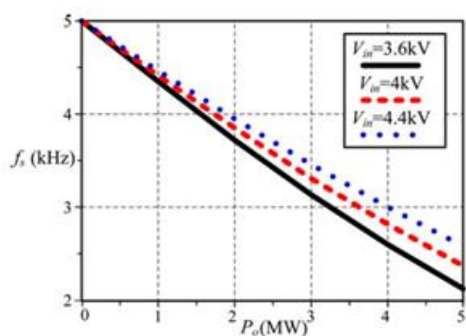


Fig. 8. Curves of switching frequency versus output power under different input voltages.

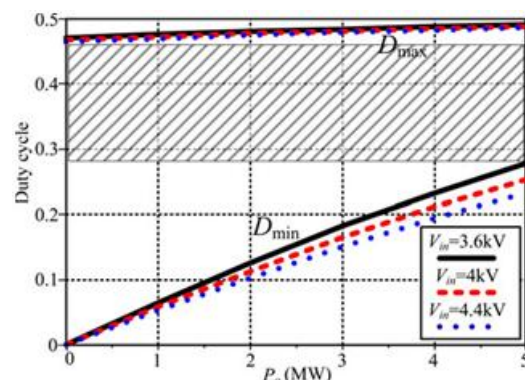


Fig. 9. Curves of  $D_{min}$  and  $D_{max}$  versus output power under different input voltages.

TABLE II  
SIMULATION PARAMETERS

Item	Symbol	Value
Input voltage	$V_{in}$	3.6–4.4 kV
Output voltage	$V_o$	80 kV
Resonant inductance	$L_r$	600 $\mu$ H
Resonant capacitance	$C_r$	1.68 $\mu$ F
Filter capacitance	$C_1, C_2$	22 $\mu$ F
Duty cycle	$D$	0.4

### III. ANALYSIS AND DESIGN OF THE CONVERTER:

#### A Voltage Rating and DC Fault Response

According to the analysis of Section II, the voltage stresses of Q1 and Q2 are the input voltage  $V_{in}$ , the voltage stresses of Q3 and Q4 are half of the output voltage, i.e.,  $V_o/2$ , the voltage stresses of Db1 and Db2 are  $V_o/2 - V_{in}$ . The total voltage stress of the primary semiconductor devices is  $2V_o$ , which is half of that in [26]–[29]. It implies that much less semiconductor devices are required in the proposed step-up converter, resulting in low conduction and switching losses and low cost. Moreover, the peak voltages across the resonant inductor and resonant capacitor are  $V_o/2$ , which is also half of that in [26]–[29]. Lower peak voltage indicates that the insulation is easy to be implemented, leading to the reduction of the size of the resonant tank. As shown in Fig. 1, the proposed converter can block an output fault and prevent the fault pass through input side, and vice versa.

The comparison of different no isolated converter topologies is listed in Table I.

### B. Voltage Balance Between C1 and C2:

The previous analysis is based on the assumption that voltages across C1 and C2 are, respectively, half of output voltage. Provided that  $V_{c1} = V_{c2}$ , for example,  $V_{c1} > V_o/2 > V_{c2}$ , according to the operation principle of Fig. 2, the peak current of icat t3 will be smaller than that at t8, which means that the average current flowing into C1 will be smaller than the average current flowing into C2. Due to C1 and C2 power the same load,  $V_{c1}$  decreases and  $V_{c2}$  increases, and finally they share the same output voltage. Vice versa, i.e.,  $V_{c1}$  increases and  $V_{c2}$  decreases under the presumption that  $V_{c1} < V_o/2 < V_{c2}$ . The previous analysis is based on the assumption that voltages across C1 and C2 are, respectively, half of output voltage. Provided that  $V_{c1} = V_{c2}$ , for example,  $V_{c1} > V_o/2 > V_{c2}$ , according to the operation principle of Fig. 2, the peak current of icat t3 will be smaller than that at t8, which means that the average current flowing into C1 will be smaller than the average current flowing into C2. Due to C1 and C2 power the same load.

### C. Analysis of the Converter:

It can be seen that the gain of  $V_o/V_{in}$  is impacted by the parameters of the resonant tank ( $L_r$  and  $C_r$ ) and the time interval of t4 to t5, which is a part of switching period; hence, in other words, the gain is impacted by  $L_r$ ,  $C_r$ , and the switching frequency. Several important conclusions are obtained For any given voltage gain (larger than 2) and the resonant tank parameters  $L_r$  and  $C_r$ , there must be a T4 to meet, which implies that for given  $L_r$  and  $C_r$ , the voltage gain can be infinite if the switching frequency range is not taken into account. For given voltage gain, the larger the  $\omega_r$ , the shorter the T4; an example is shown in Fig. 5, which means that the switching frequency will be higher. For given voltage gain and  $\omega_r$ , although T4 is constant, but the expressions of T1, T2, and T3 are related to  $L_r$  and  $C_r$ , which means that different pairs of  $L_r$  and  $C_r$  impact the switching frequency of the proposed converter.

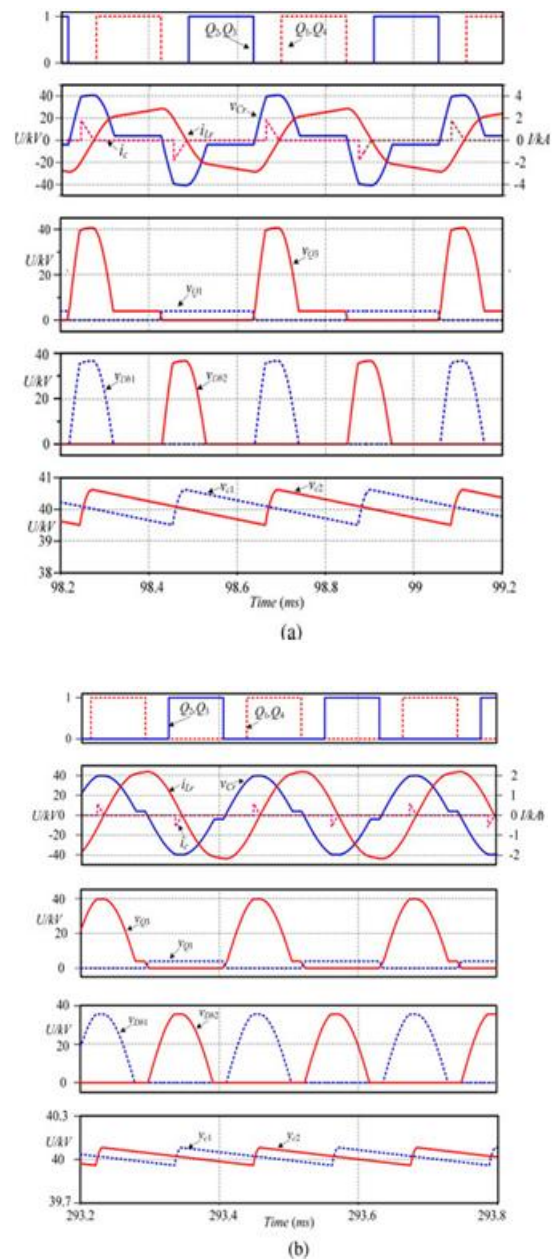


**Fig. 10. Steady-state simulation results under different load conditions when  $V_{in} = 4$  kV. (a) 5 MW. (b) 1 MW.**

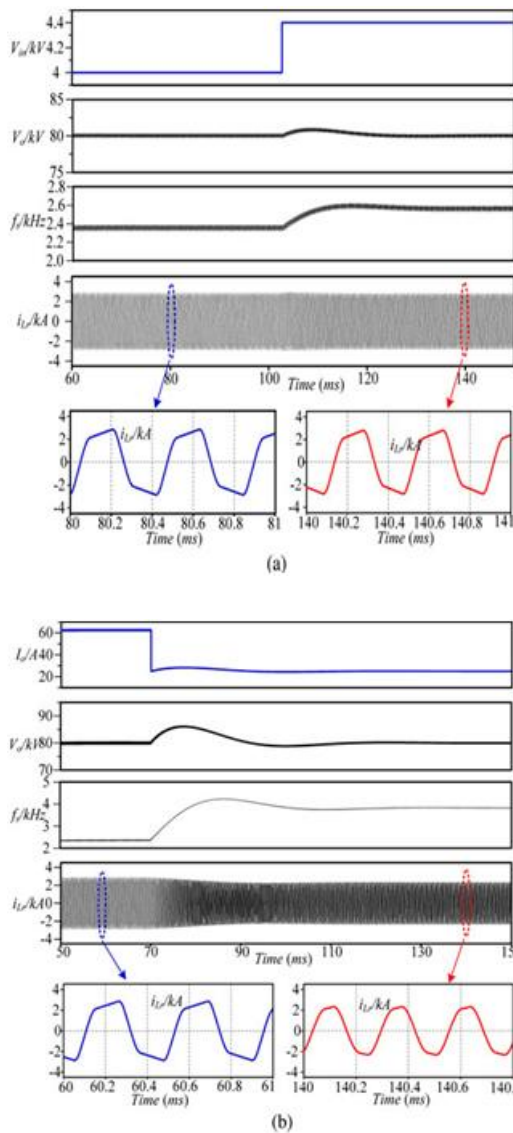


Fig. 11. Dynamic simulation results. (a) Input voltage step. (b) Load step.

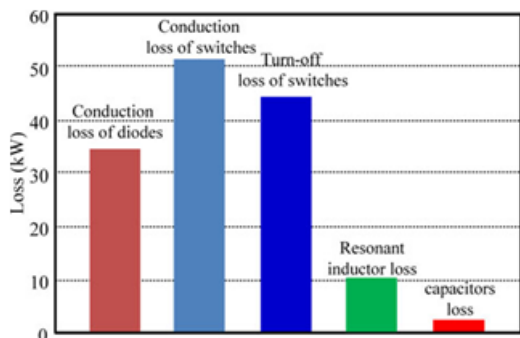


Fig. 12. Calculated power losses distribution.

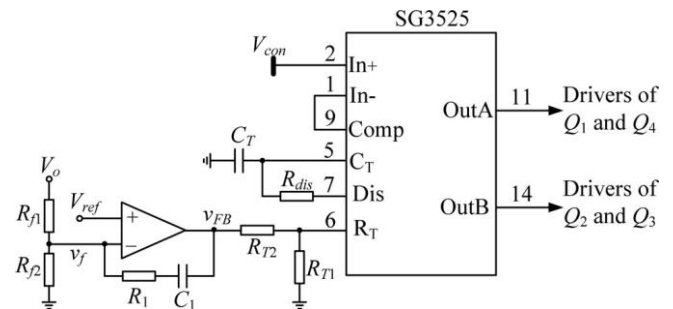
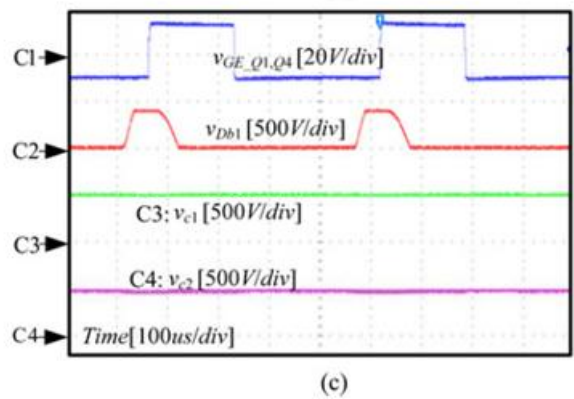
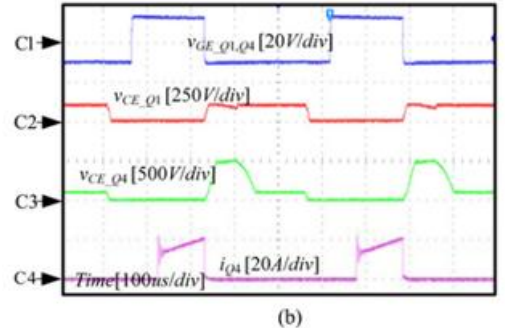
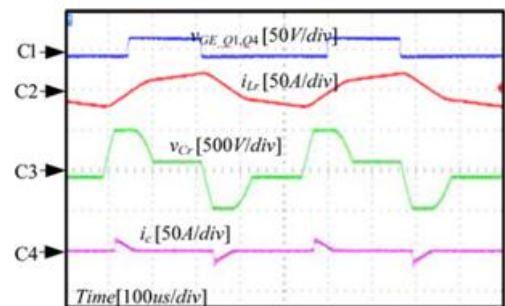
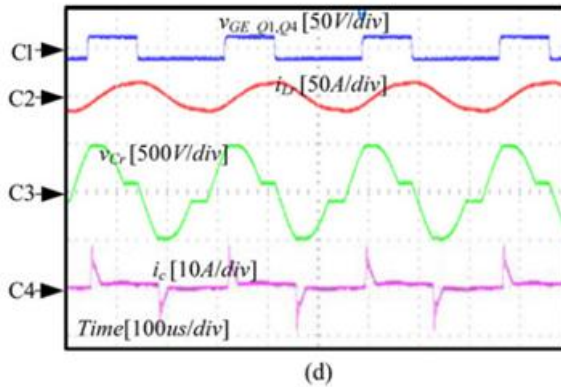


Fig. 13. Block diagram of the control circuit.





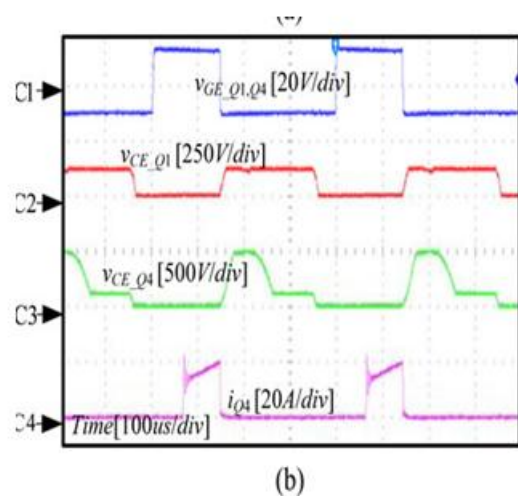
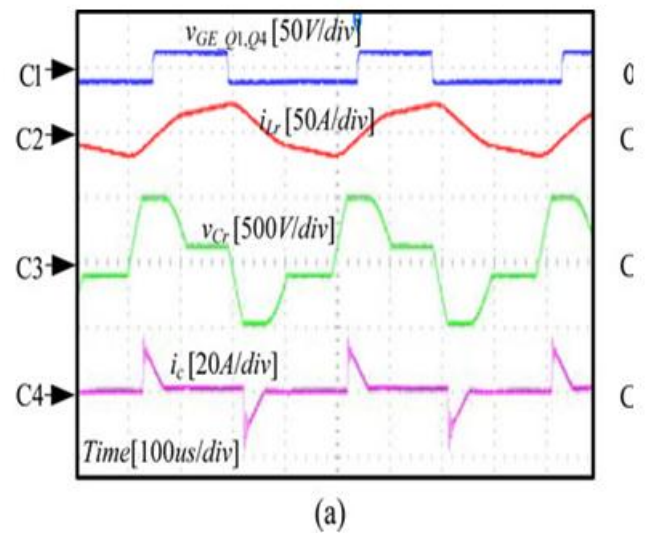
**Fig. 14. Experimental waveforms under (a)–(c) 1 kW and (d)–(f) 200 W load conditions when  $V_{in} = 100$  V. (a), (d)  $v_{GE}$  of  $Q_1$ , current of  $L_r$ , voltage across  $C_r$  and  $i_c$ . (b), (e)  $v_{GE}$  of  $Q_1$ ,  $v_{CE}$  of  $Q_1$ ,  $v_{CE}$  of  $Q_4$ , and current of  $Q_4$ . (c), (f)  $v_{GE}$  of  $Q_1$ , voltage across  $D_{b1}$ , and voltages across  $C_1$  and  $C_2$**

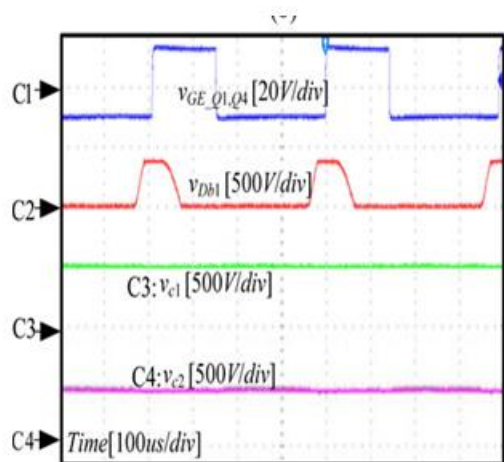
Can be the any value in the range of 0.277–0.465, as the shaded area shown in Fig. 9. Therefore, the control of the proposed converter is very simple with constant duty cycle and variable switching frequency.

#### IV. SIMULATION AND EXPERIMENTAL RESULTS

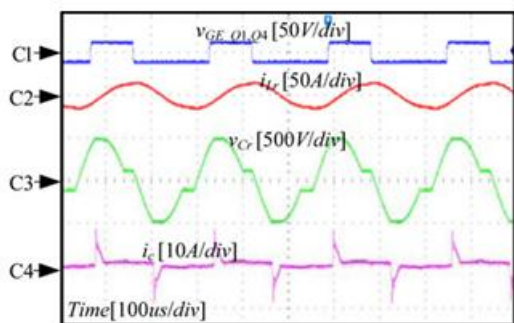
In order to verify the operation principle and the theoretic-cal analysis, a converter is simulated with PLECS simulation software and the detailed parameters are listed in Table II. All switches used in PLECS simulation are ideal switches and 5 nF capacitance is added in parallel with  $D_{b1}$  and  $D_{b2}$ . Fig. 10 shows the simulation results at the output power of 5 and 1 MW ( $V_{in} = 4$  kV), respectively. As the figure shows, the voltage stress of  $Q_1$  and  $Q_2$  is 4 kV, the voltage stress of  $Q_3$  and  $Q_4$  is 40 kV, the voltage stress of  $D_{b1}$  and  $D_{b2}$  is 36 kV, and the peak voltage across the LC resonant tank is 40 kV.  $Q_1$  through  $Q_4$  are turned on under zero-voltage condition and when they are turned off, the voltage across the device increases slowly from zero. The switching frequencies of the converter at 5 and 1 MW are 2.3 and 4.4 kHz, respectively. The simulation results match well with the aforementioned analysis.

Fig. 11(a) illustrates the simulation results corresponding to a step change of input voltage from 4 to 4.4 kV under full-load condition. It can be seen that the output voltage is regulated to be constant and the switching frequency  $f_s$  changes from 2.3 to 2.5 kHz. Fig. 11(b) illustrates the simulation results corresponding to a load stepping from full load to 40% load under 4 kV input voltage condition. It can be seen that the output voltage is regulated to be constant and the switching frequency  $f_s$  changes from 2.3 to 3.8 kHz. The simulation results match well with Fig. 8 and the control strategy of variable frequency with constant duty cycle is validated.

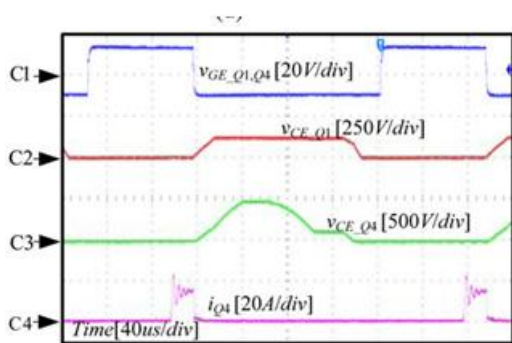




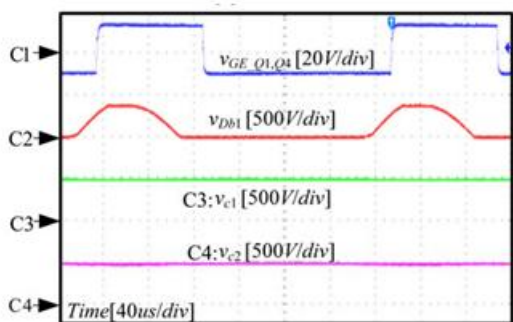
(c)



(d)



(e)



(f)

**Fig. 15. Experimental waveforms under (a)–(c) 1 kW and (d)–(f) 200 W load conditions when  $V_{in} = 120$  V. (a), (d)  $v_{GE}$  of Q1, current of  $L_r$ , voltage across  $C_r$  and  $i_c$ . (b), (e)  $v_{GE}$  of Q1,  $v_{CE}$  of Q1,  $v_{CE}$  of Q4, and current of Q4. (c), (f)  $v_{GE}$  of Q1, voltage across  $Db1$ , and voltages across  $C1$  and  $C2$ .**

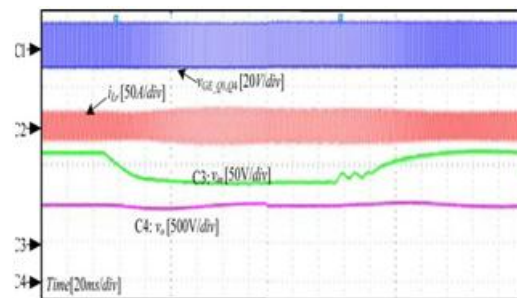


**Fig. 16. Experimental waveforms of an input voltage step change.**

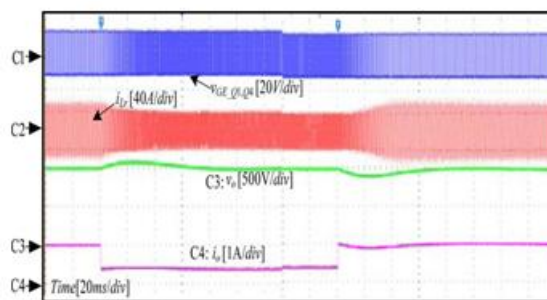


**Fig17. Experimental Waveform Of Load Step Change .**

The effectiveness and misfortunes dissemination of the 5 MW condition is additionally computed. HiPak IGBT module 5SNA 0600G650100 (6500 V, 600 A) from ABB is utilized as the dynamic switches. In the count, ten 6500 V IGBTs are associated in arrangement to hold up 40 kV. HiPak diode module 5SLD 0600J650100 (6500 V, 1200 A) from ABB is utilized as the information blocking diodes and rectifier diodes. The center material of the resounding inductor is VITROPERM 500 F. Reasonable high-voltage capacitors are looked over EACO. The figured proficiency is around 97.2% and the misfortunes dispersion is delineated in Fig. 12. It can be watched that the prevailing part of the force misfortunes is the conduction loss of diodes and switches.

In spite of the fact that the turn-on misfortune is killed because of zero-voltage turn-on condition, as a result of the tail current trademark, the turn-off loss of the IGBTs must be eased on account of the moderate expanding of the voltage over the dynamic switch. In the event that the high-voltage vast current silicon carbide (SiC) MOSFET is accessible later on [24], the turn-off loss of the converter could be decreased significantly. In request to check the operation of the proposed converter, a 100 V ( $\pm 20\%$ )/1000 V, 1 kW model converter was implicit our research facility. The parameters are  $L_r = 1200 \mu\text{H}$ ,  $C_r = 0.8 \mu\text{F}$ ,  $C_1 = C_2 = 150 \mu\text{F}$ , Q1–Q4 are FF200R17KE3, the antiparallel diodes of other FF200R17KE3 are taken as the Db1 and Db2, and rectifier diode is DSDI60-18A. The main control block of the proposed converter is shown in Fig. 13. The conventional pulse width modulation control IC SG3525 is used with variable frequency operation. A constant voltage is connected to Pin 2 to determine a constant duty cycle. The oscillator frequency of the SG3525 is determined by the  $R_T$  and  $C_T$ , which are connected to Pin 6 and Pin 5, respectively.

Hence, by connecting an external resistor ( $R_{T2}$ ) to Pin 6 with a variable voltage ( $V_{FB}$ ), a voltage controlled oscillator is obtained and the variable frequency constant duty cycle modulation is realized. According to Fig. 8, the output power of the converter is decreased with the increase of the switching frequency. Hence, the stable output voltage regulation process of the variable frequency controller can be expressed as  $V_o \uparrow \rightarrow v_f \uparrow \rightarrow v_{FB} \downarrow \rightarrow f_s \uparrow \rightarrow P_o \downarrow \rightarrow V_o \downarrow \rightarrow V_o \text{ constant}$ . Fig. 14 shows the experimental waveforms of the converter under 1 kW and 200 W conditions with 100 V input voltage, respectively.

Fig. 15 shows the experimental waveforms of the converter under 1 kW and 200 W conditions with 120 V input voltage, respectively. As Fig. 14 shows, the voltage stress of Q<sub>1</sub> is 100 V, the voltage stress of Q<sub>4</sub> is 500 V, the voltage stress of D<sub>b1</sub> is 400 V, and the peak voltage across the LC resonant tank is 500 V.

The collector–emitter voltages  $V_{CEQ1}$  and  $V_{CEQ4}$  have been zero when Q<sub>1</sub> and Q<sub>4</sub> are turned on; hence, they are turned on with zero voltage. The increase of  $V_{CEQ4}$  is slow when Q<sub>4</sub> is turned off; hence, it is turned off with almost zero voltage. The oscillation of  $i_{Q4}$  is caused by the parasitic inductor of the prototype. All the waveforms agree well with the expected switching sequence in Fig. 2. Fig. 16 illustrates the output voltage corresponding to a step change of input voltage varying between 80 and 120 V. Fig. 17 illustrates the output voltage corresponding to a step change of load current varying between 1 and 0.4 A. As seen, the output voltage can be regulated to be constant corresponding to the input voltage step change and load step change. Fig. 18 shows the conversion efficiency of the proposed converter. Fig. 18(a) shows the efficiency at different output currents under normal input voltage of 100 V. Fig. 18(b) shows the efficiency at full load under different input voltages. It is shown that the maximum efficiency can be up to 95.2%.

As Fig. 18(a) shows, the efficiency decreases with the decrease of the output power, because the switching frequency is higher at light load than that at heavy load (see Fig. 8), so the turn-off loss of switches increases at light load and is the main part of the loss. For the constant output power, the average input current decreases with the increase of the input voltage; hence, the conduction loss will decrease with the increase of the input voltage. However, the switching frequency increases with the increase of the input voltage (see Fig. 8); hence, the switching loss (turn-off loss) will increase with the increase of the input voltage. So, there is an optimum efficiency working point in the input voltage range, as shown in Fig. 18(b).

## V. CONCLUSION:

A novel thunderous dc–dc converter is proposed in this paper, which can accomplish high stride up voltage addition and it is suit-capable for high-control high-voltage applications. The converter uses the thunderous inductor to convey power by charging from the information and releasing at the yield.

The thunderous capacitor is utilized to accomplish zero-voltage turn-on and turn-off for the dynamic switches and ZCS for the rectifier diodes. The examination exhibits that the converter can work at any addition esteem ( $> 2$ ) with appropriate control; in any case, the parameters of the thunderous tank decide the greatest exchanging recurrence, the scope of exchanging recurrence, and current appraisals of dynamic switches and diodes. The converter is controlled by the variable exchanging recurrence. Reproduction and exploratory results check the operation rule of the converter and parameters determination of the thunderous tank.

## REFERENCES:

- [1] CIGRE B4-52 Working Group, HVDC Grid Feasibility Study. Melbourne, Vic., Australia: Int. Council Large Electr. Syst., 2011.
- [2] A. S. Abdel-Khalik, A. M. Massoud, A. A. Elserougi, and S. Ahmed, "Optimum power transmission-based droop control design for multi-terminal HVDC of offshore wind farms," *IEEE Trans. Power Syst.*, vol. 28, no. 3, pp. 3401–3409, Aug. 2013.
- [3] F. Deng and Z. Chen, "Design of protective inductors for HVDC transmission line within DC grid offshore wind farms," *IEEE Trans. Power Del.*, vol. 28, no. 1, pp. 75–83, Jan. 2013.
- [4] F. Deng and Z. Chen, "Operation and control of a DC-grid offshore wind farm under DC transmission system faults," *IEEE Trans. Power Del.*, vol. 28, no. 1, pp. 1356–1363, Jul. 2013.
- [5] C. Meyer, "Key components for future offshore DC grids," Ph.D. dissertation, RWTH Aachen Univ., Aachen, Germany, pp. 9–12, 2007.
- [6] W. Chen, A. Huang, S. Lukic, J. Svensson, J. Li, and Z. Wang, "A comparison of medium voltage high power DC/DC converters with high step-up conversion ratio for offshore wind energy systems," in *Proc. IEEE EnergyConvers. Congr. Expo.*, 2011, pp. 584–589.
- [7] L. Max, "Design and control of a DC collection grid for a wind farm," Ph.D. dissertation, Chalmers Univ. Technol., Goteborg, Sweden, pp. 15–30, 2009.
- [8] Y. Zhou, D. Macpherson, W. Blewitt, and D. Jovicic, "Comparison of DC-DC converter topologies for offshore wind-farm application," in *Proc. Int. Conf. Power Electron. Mach. Drives*, 2012, pp. 1–6.
- [9] S. Fan, W. Ma, T. C. Lim, and B. W. Williams, "Design and control of a wind energy conversion system based on a resonant dc/dc converter," *IET Renew. Power Gener.*, vol. 7, no. 3, pp. 265–274, 2013.
- [10] F. Deng and Z. Chen, "Control of improved full-bridge three-level DC/DC converter for wind turbines in a DC grid," *IEEE Trans. Power Electron.*, vol. 28, no. 1, pp. 314–324, Jan. 2013.
- [11] C. Meyer, M. Hoing, A. Peterson, and R. W. De Doncker, "Control and design of DC grids for offshore wind farms," *IEEE Trans. Ind. Appl.*, vol. 43, no. 6, pp. 1475–1482, Nov./Dec. 2007.
- [12] C. Meyer and R. W. De Doncker, "Design of a three-phase series resonant converter for offshore DC grids," in *Proc. IEEE Ind. Appl. Soc. Conf.*, 2007, pp. 216–223.
- [13] S. P. Engel, N. Soltan, H. Stagge, and R. W. De Doncker, "Dynamic and balanced control of three-phase high-power dual-active bridge DC-DC converters in DC-grid applications," *IEEE Trans. Power Electron.*, vol. 28, no. 4, pp. 1880–1889, Apr. 2013.
- [14] K. Stephan, "Modular DC/DC converter for DC distribution and collection networks," Ph.D. dissertation, EPFL, Lausanne, Switzerland, pp. 81–94, 2012.
- [15] T. Luth, M. Merlin, T. Green, F. Hassan, and C. Barker, "High frequency operation of a DC/AC/DC system for HVDC applications," *IEEE Trans. Power Electron.*, vol. 29, no. 8, pp. 4107–4115, Aug. 2014.
- [16] Y. Zhou, D. Jiang, P. Hu, J. Guo, Y. Liang, and Z. Lin, "A prototype of modular multilevel converters," *IEEE Trans. Power Electron.*, vol. 29, no. 7, pp. 3267–3278, Jul. 2014.
- [17] W. Chen, X. Ruan, H. Yan, and C. K. Tse, "DC/DC conversion systems consisting of multiple



converter modules: Stability, control and experimental verifications,” IEEE Trans. Power Electron., vol. 24, no. 6, 1463–1474, Jun. 2009.

[18]K. Park and Z. Chen, “Analysis and design of a parallel-connected single active bridge DC-DC converter for high-power wind farm applications,” in Proc. Eur. Conf. Power Electron. Appl., 2013, pp. 1–10.

[19]C. Zhan, A. Bullock, C. Smith, and A. Crane, “Power collection and transmission systems,” Eur Patent Appl., EP2341594A1, 2011.

[20]P. Monjean, J. Delanoe, J. Auguste, C. Saudemont, J. Sprooten, A. Mirza-ian, and B. Robyns, “Topologies comparison of multi-cell medium frequency transformer for offshore farms,” in Proc. Int. Conf. AC DC PowerTransmiss., 2010, pp. 1–5.